Lab manual: Single-photon detector

Mikhail Petrov, Elena Anisimova, and Vadim Makarov
(Dated: November 23, 2023)

I. OBJECTIVES

This lab exercise teaches the properties and characterisation of a single-photon detector (SPD), including measurement of its dark count rate, photon detection efficiency, dead time, and saturation. During the exercise the students learn to operate laboratory instruments (oscilloscope, power meter, counter, etc.) and manipulate fiber-optic components.

II. PREREQUISITES AND OUTLINE

This lab exercise requires background knowledge about a single-photon detector built around an InGaAs/InP avalanche photodiode (APD) for the detection of near-infrared single photons. An overview of modern types of SPDs along with their characterisation methods (one of which you will use in this work) is presented in R. Hadfield's review article [1], providing a good background reading. Please do not skip it, as it is an essential part of the preparation.

Surprisingly, article [1] contains a minor error in the last equation in Box 1 (last equation on page 697). This is the equation you probably have to use for your work. As part of your preparation, find the error and correct it.

A. Outline

During the lab you will learn how to operate an APD-based single-photon detector and characterise it, measuring the following parameters.

1. Dark count rate (DCR).

2. Photon detection efficiency.

3. Dead time, maximum count rate, and saturation.

B. Questions for preparation

– Explain the mechanism of detection of single photons by APDs.

– What mechanisms are causing dark counts in APDs?

– Explain how to measure DCR.

– What is a standard deviation, how do you calculate it, and what notation do you use to report it in the results?

– What is SPD's dead time? How does it correlate with the maximum count rate? How to measure both parameters?

– How to measure the quantum efficiency? Draw a scheme.

– What should be the mean photon number μ per laser pulse to get non-empty pulses contain one photon with 80% probability (while the other non-empty pulses contain two or more photons)?

III. THEORY

A. Single-photon detectors

Several technologies for single-photon detection are available on the market [1]. They demonstrate a wide range of parameters, such as the wavelength range in which the detector is sensitive, the size of its photosensitive area, its dark count rate, efficiency, timing jitter, afterpulsing, and other properties.

B.   Avalanche photodiode

In this lab exercise you will characterise an SPD based on InGaAs/InP reverse-biased APD.

Avalanche photodiodes are able to register light due to the photoelectric effect that converts light to electricity. Their design provides an in-built gain mechanism through an avalanche multiplication process. To be used for the single photon counting, a reverse bias voltage applied to the APD is set above APD's breakdown voltage [2]. Then the APD is either in a quiescent state with negligible current or in a state with a self-sustaining avalanche breakdown. The avalanche process can be triggered by a single carrier, either thermally excited or resulting from ionization by a photon.

To provide quenching for this avalanche current, a high-impedance load (usually a resistor) can be connected between the APD and the bias voltage source. The avalanche current self-quenches simply because it develops a voltage drop across a high-value ballast load. This is called a passive quenching method. After the avalanche quenched, the APD restores into its zero-current state, and the voltage across the diode starts recovering up to its initially set value. The period after the avalanche has stopped and until an APD is able to produce the next avalanche is called a dead time.

To minimize the dead time and operate the device at a faster rate, an active quenching circuit can be implemented [2, 3]. A special electronic circuit detects the occurrence of the avalanche and then reduces the bias voltage applied at the APD, thereby interrupting the avalanche. The quenching transition is forced a few nanoseconds after the avalanche is triggered, and the APD can be held off for a preset time ranging from tens of nanoseconds to tens of microseconds [2, 3]. In this lab we study the SPD with active quenching.

Dark counts in APDs are mostly caused by thermally exited carriers that trigger avalanches in the absence of any light. Cooling the APD decreases the thermal energy of carriers, thus the DCR decreases with temperature. Another important source of dark counts are carriers trapped in metastable impurity levels during the previous avalanche. These carriers release at random and can cause a count called an afterpulse if the bias voltage is raised too soon after the avalanche. Lengthening the dead time allows most of these trapped carriers to dissipate without causing the avalanche, thus decreasing the afterpulse probability.

C.   Main parameters of SPDs

- **Dark count rate** is the mean rate of false counts or noise of the SPD. They arise through different mechanisms depending on the SPD's structure and materials. E.g., in APDs most of the dark counts are caused by thermal excitation and depend on temperature of APDs; in photomultiplier tubes dark count pulses originate from thermal emission of electrons from the photocathode and dynodes; in superconducting nanowire SPDs dark counts caused by intrinsic processes are extremely low, can be less than 10^{-4} Hz.

  Dark counts in receivers introduce errors in quantum communications. In quantum key distribution (QKD), the dark counts increase an error rate and reduce the amount of distillable secret key. In quantum teleportation, dark counts affect data collection time needed to verify the quality of the teleportation. Too many dark counts lead to the communication protocol failing to work at all.

- **Detection efficiency** is the probability of creating an output click when a photon hits the sensitive area of the detector. Not all photons arriving at the SPD get detected, owing to various optical and electronic loss mechanisms. The highest detection efficiency over 98% at 1550 nm has been reported for a superconducting nanowire single-photon detector (SNSPD) [4]. For Si APDs at visible wavelengths, higher than 50% efficiency is routinely available in commercial products.

  Higher detection efficiency in QKD increases the key rate.

- **Timing jitter** describes a fluctuation of the time delay between the photon impinging the SPD and the output pulse appearing. While the absolute length of delay is not important, its random fluctuation from one detection to another is. The latter is usually measured by the full-width at half-maximum (FWHM) of the delay's timing histogram, built over many identical detections of a very short optical pulse. It varies from 15 ps (for SNSPDs) to 300–400 ps (for larger-size APDs and PMTs).

  The timing jitter is limiting the time resolution and clock rate in communication systems.

- **Afterpulses** are noise counts that appear after a registered count and are caused by intrinsic processes in some types of SPDs. In APDs afterpulses are caused by carriers trapped during an avalanche, then spontaneously released and triggering a new avalanche.

  In quantum communications, afterpulsing in SPDs leads to errors. It can be suppressed by a sufficiently long dead time or discarded during post-processing.

- **Maximum count rate** determines the maximum number of photons per second that the SPD is able to count. APDs have a dead time (recovery time) after each avalanche, during which they are unable to register photons. The highest count rate of 16.7 GHz has been reported for SNSPDs working in 250–340 nm range.

- **Diameter of detector's sensitive area** allows it to be integrated with different types of communication systems. Fiber-optic systems carry light in a 9 µm diameter fiber core, allowing efficient optical coupling with very small detectors of about 20 µm size. The APD studied in this lab is one of these small fiber-coupled devices. However, free-space communication systems where light travels through a turbulent atmosphere and becomes spread over different incoming directions cannot focus it in a small area. They require detector photosensitive area of 100 to 500 µm diameter for efficient photon collection [5]. Fabricating larger SPDs is challenging, because the size of the device strongly affects all the other parameters and multiplies the amount of imperfections and undesirable effects. Most technologies allow devices no larger than a fraction of a millimeter. The only type of SPD available with a huge photosensitive surface (centimeters or larger) is a photomultiplier tube, but it has limitations and is rarely used in quantum communication systems.

D. Photon statistics

Photon statistics is the theoretical and experimental study of the statistical distributions produced in photon counting experiments, which use photodetectors to analyze the intrinsic statistical nature of photons from a light source. In this lab exercise, you will use strongly attenuated laser pulses to get single photons for the SPD test. The photon number distribution for such sources is described by Poissonian statistics.

Poissonian distribution of the photon number per laser pulse is given by

$$P(k) = \frac{\mu^k e^{-\mu}}{k!}, \tag{1}$$

where $k = 0, 1, 2, ...$ is an integer photon number in a laser pulse,
μ is an average photon number per pulse (μ is a non-negative real number),
and $P(k)$ is the probability to have k photons in a laser pulse at a given μ.

IV. EQUIPMENT

1. Educational system made by QRate, unit Bob. Includes: laser SWLD 1554.94-FC/PC-10PM with driver electronics, SPD developed by QRate (based on an InGaAs/InP APD), computer with control software installed.

2. Optical power meter Thorlabs PM400 with S155C fiber-optic photodiode power sensor.

3. Oscilloscope LeCroy SDA816Zi (or a similar model).

4. Optical-to-electrical converter LeCroy OE-555 (or a similar model).

5. Electronic counter Stanford Research Systems SR620.

6. Two fiber-optic programmable attenuators Grandway FHA2S02 (or a similar model).

7. Fiber-optic fixed attenuators Thorlabs FAXXT, where XX is approximate amount of attenuation in dB.

8. High-brightness non-directional wideband infrared light source (an incandescent lamp).

9. Cables and adapters.

10. Fiber cleaning kit.

11. Black cloth.

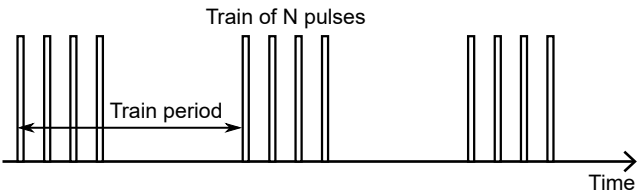The operator's manuals for the equipment can be found on the course webpage.

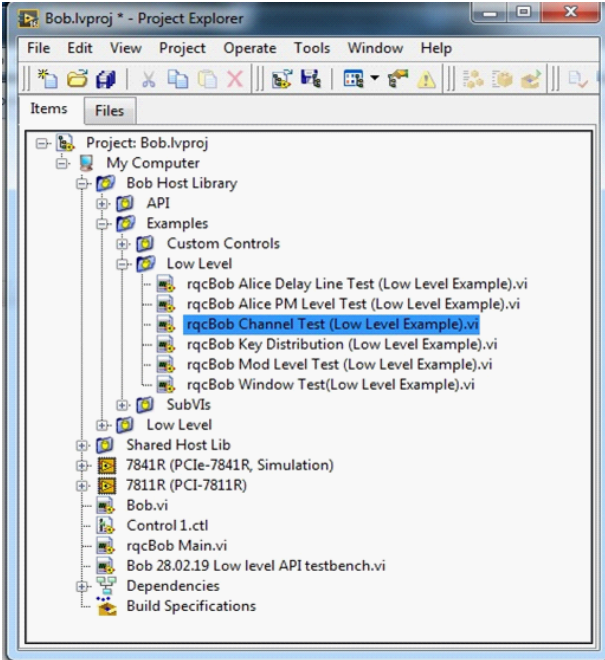FIG. 1. Trains of laser pulses emitted from QRate laser module.

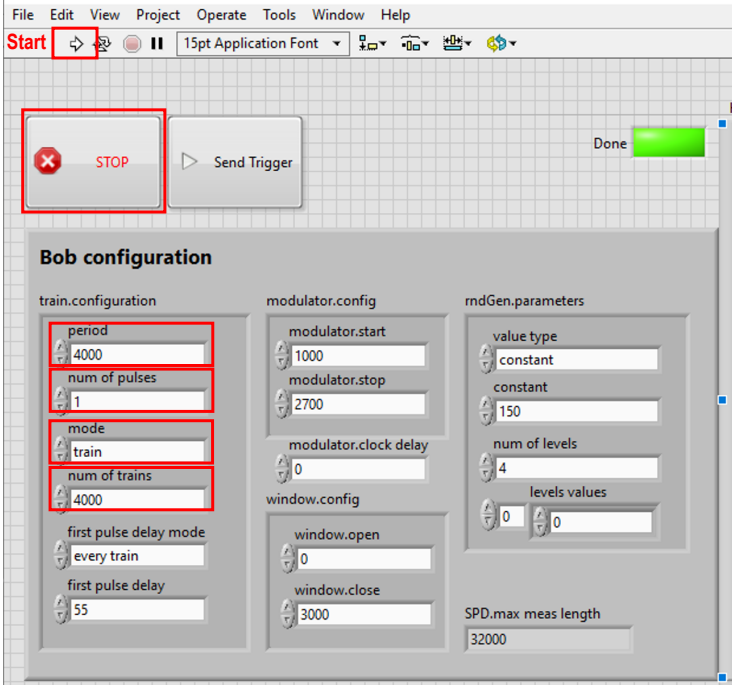FIG. 2. Starting the laser control software (rqcBob Channel Test.vi program).

FIG. 3. Laser configuration dialog in QRate system.

V.   WORKFLOW

In this lab exercise, you will use a QRate laser and detector with an electronic control system. The control system and the laser module allows to generate a packet of identical short (4–5 ns) optical pulses, which QRate calls a train (Fig. 1). While the pulse period within the train is fixed at 200 ns, the control software allows to set the number of pulses in the train, the repetition period of the trains (in units of 200 ns), and the total number of trains to be emitted during a single software run. To launch the software module controlling the laser, one should run Bob.lvproj project file on the desktop. In the dialog box that appears (Fig. 2), run the file: \Bob Host Library\Examples\Low Level\rqcBob Channel Test (Low Level Example).vi. The laser configuration dialog is shown in Fig. 3, with relevant controls highlighted by red rectangles.

1. **Preparation of an attenuated laser source**

   (a) Power on the computer, QRate educational system, oscilloscope, and counter.

   (b) Connect the oscilloscope to the laser output via the optical-to-electrical converter. Observe the laser pulses, check their shape, width, record oscillograms.

   Here you should take into consideration that the optical-to-electrical converter has a limited linear range. If its peak input optical power is too high, it will saturate and distort the pulse shape recorded at the oscilloscope. An optical attenuator (either fixed or programmable one) can be used to reduce the optical power.

   Another pitfall with this optical-to-electrical converter is that the oscilloscope software defaults on using a bandwidth-limiting filter ("reference receiver" in the probe configuration menu). If you want to see the real pulse shape at the full converter bandwidth, you must disable this filter in the configuration menu. See the operator's manual for the converter if you have questions.

   (c) Connect the optical power meter to the laser output, measure the laser output optical power. This power meter measures optical power averaged over a relatively long time, not peak power of individual pulses.

   (d) Record the output optical power for different train repetition rates and different number of pulses in the train.

   (e) Calculate the mean number of photons per pulse.

   (f) Calculate how much optical attenuation needs to be applied in order to get the mean output photon number per pulse $\mu = 0.2$.

   Lab report should contain: diagram of your experimental setup, laser pulse oscillograms, optical power measurement results, conditions of the measurement, equation for photon number calculation, photon number calculation results, and any observations and explanations you deem relevant.

2. **Operation of the SPD and measurement of its DCR**

   Dark counts will be observed via the oscilloscope and measured by the counter.

   (a) Connect SPD USB out to the PC USB port, run software module SPD_Client (on the desktop) and check that the SPD has cooled down to its operating temperature and ready.

   (b) Connect the oscilloscope to the SPD output, observe output pulses, check their shape, record oscillograms. Estimate the DCR from the oscillogram (select a time scale that shows you a sufficient number of pulses in one oscillogram to count them and obtain a meaningful estimate of the count rate).

   (c) Connect the counter to the SPD output simultaneously with the oscilloscope and compare its reading (taken with measurement time of 1 s) with results for DRC from (b). Note that a simultaneous connection of the SPD output to two instruments requires a correct cable configuration and impedance matching, to avoid reflections and signal distortion in the coaxial cables.

   (d) Check if the incandescent lamp or any other bright light source directed at the SPD optical input socket without a cap induces any changes in the result.

   (e) Check if a complete black-out induces any changes in the result (use a metal cap at the detector input and the black cloth to cover the detector, shielding it completely from the ambient light).

(f) Do the DCR measurement with the counter, setting the measurement time at 100 s. Compare your result with the estimates you did in (b) and (c). In SR620, the actual gate time for the internal gates is the gate time set on the front panel multiplied by the "gate scale" set in the output configuration menu (see SR620 operator's manual, p. 18). Thus if one desires a 100 s gate, one would set the gate scale at 100 and select 1 s gate time on the front panel (1 s × 100 = 100 s).

(g) Calculate the uncertainty of your last DCR measurement. Please use a parenthesis notation to denote the standard (i.e., one-sigma) uncertainty in the measured value [6]. Note that a simple theoretical estimate of the uncertainty will suffice. An attempt at its experimental verification is not required.

Here is an example. Suppose you count the dark detector clicks for 100 s and obtain 12459 clicks. The dark count rate $D = 12459/100$ s ≈ 124.6 Hz. We know from the detector physics that its counts are mostly a Poisson process, i.e., they occur with the same probability over time and each click does not depend on the previous ones [7] (here we neglect secondary effects in the detector like deadtime, afterpulses, and saturation). For a Poisson process that results in a more than a few clicks in a time period, the distribution of the number of these clicks around the true mean is Gaussian, with its one-sigma deviation being the square root of the number of events counted in the time period. I.e., the theoretical standard deviation of your measurement over 100 s is $\sqrt{12459} \approx 112$ or, when normalised to 1 s, $\sigma_D = 112/100$ s ≈ 1.1 Hz.

The result may be recorded as $D = 124.6 \pm 1.1$ Hz. In the concise parenthesis notation [6], it is stated as $D = 124.6(11)$ Hz. The number in parentheses is the numerical value of the standard uncertainty referred to the corresponding last digits of the quoted result.

What does the standard uncertainty mean? It means that the true dark count rate, which you would get if you measured for an infinite (or very long) time, lies with 68% probability between $(D - \sigma_D)$ and $(D + \sigma_D)$, i.e., between 123.5 and 125.7 Hz [8]. If you want a higher than 68% probability of the true rate being within the interval, you have to take a wider interval, e.g., $\pm 2\sigma_D$ interval for 95% probability or $\pm 3\sigma_D$ interval for 99.7% probability. In the latter case, the true dark count rate is between 121.3 and 127.9 Hz with 99.7% probability, and with 0.3% probability outside this interval, which is high enough confidence for most practical measurements. Note that even as you have counted more than 10000 clicks—which may sound as a lot to you—the statistical error of the measurement at a decent confidence level is significant, a few percent of the measured value.

Lab report should contain: diagram of your experimental setup, oscillograms, DCR measurement results with their uncertainty, explanation of the observed effects.

3. **Measurement of SPD dead time and saturation measurement**

(a) Measure the SPD dead time using the oscilloscope. We recommend that you first use a persistence display mode to roughly evaluate the behaviour of the detector output signal. Set the oscilloscope to the persistence mode, through the menu Display → Persistence setup → Persistence On, Persistence Time Infinite (see the oscilloscope manual p. 82). In Figure 4, you can see an example of the oscilloscope screen with multiple traces accumulated. The visible density of traces shows you where the pulses occur more often, or do not occur at all.

However, to obtain a quantitative measurement, we need to plot photon detection probability versus time elapsed since the last detection. This can be plotted in the oscilloscope software using its advanced signal processing capabilities. We first set up a measurement of "Time at level" on our oscillogram (see p. 92 in the oscilloscope manual and Fig. 5). We then histogram the results of this measurement (see p. 99 in the oscilloscope manual and Fig. 6). Note that, in order to get a nice histogram, you need to change some of its parameters as shown in Fig. 6. You can then sit and wait until the histogram accumulates enough counts for an acceptable signal-to-noise ratio, so that it looks at least as smooth as the one in Fig. 6. This data acquisition can be significantly sped up by switching the oscilloscope into a "sequence" sampling mode, because it will then acquire multiple oscillograms into its waveform memory and update the screen infrequently to save processing time (see p. 45 of the oscilloscope manual). Illuminating the detector slightly with the incandescent lamp also helps, as it increases the count rate. However be careful not to overdo this and drive it into a saturation, as the histogram would look very different then.

From your histogram, you can determine the dead time. Most likely, you will notice that the recovery from the dead time is a gradual process. A few counts appear early on, the sensitivity rises gradually, and may even peak before it settles to a steady value. You should therefore think how you define the dead time.

(b) Connect the attenuated light source (with the programmable attenuator) to the optical input of the SPD. Keep the output of the SPD connected to the oscilloscope and counter. Since we will be checking the
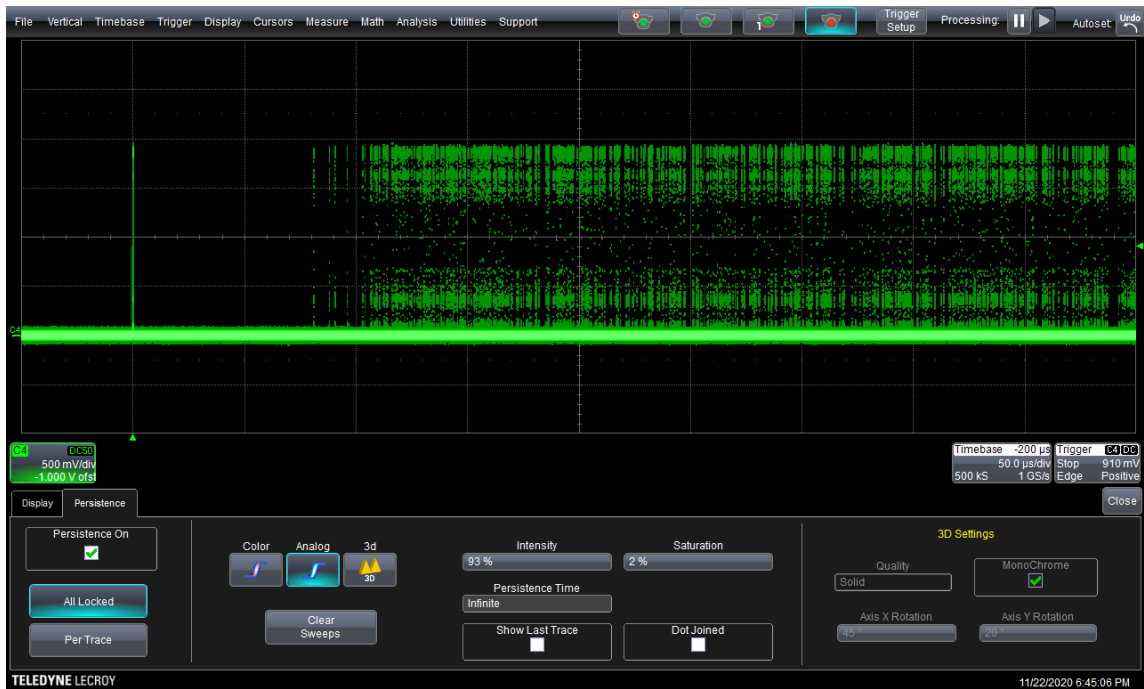
FIG. 4. An example of the oscilloscope screen with an oscillogram of detector output in persistence mode, showing the recovery of sensitivity after a click.

FIG. 5. A measurement is set up on the oscillogram to measure time of a pulse since trigger. A gate is set up to exclude the triggering pulse from the measurement.
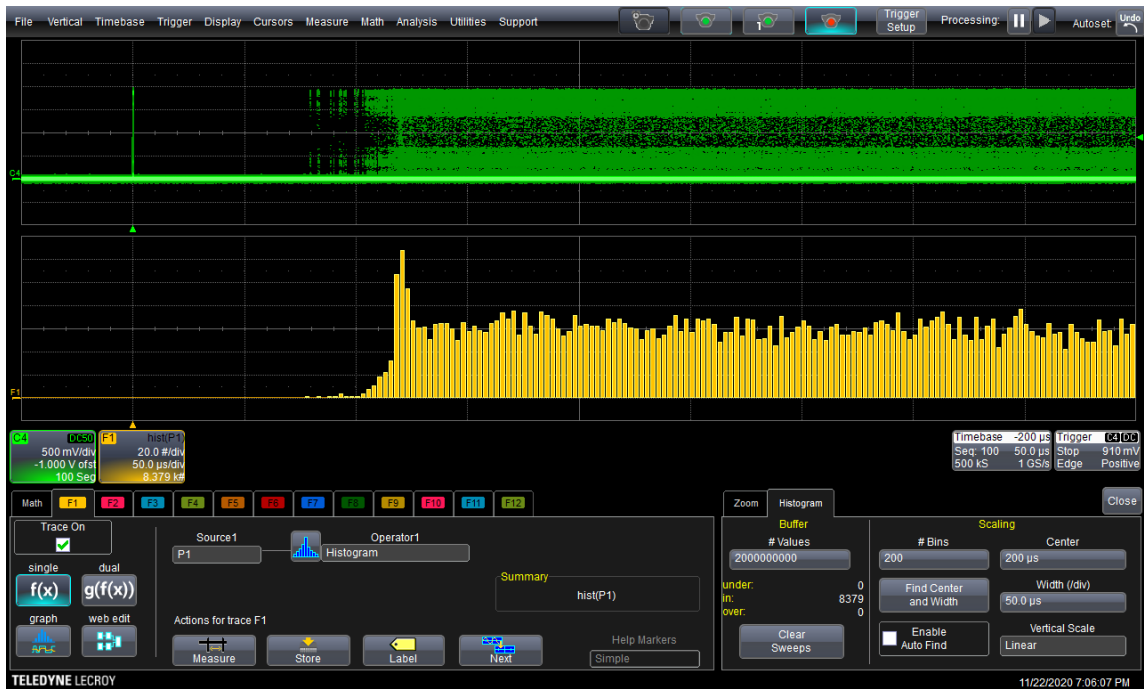
FIG. 6. A histogram of the time measurement shows how the detector recovers from the deadtime. We see a gradual transition from zero to nominal photon detection probability, with a peak in-between that possibly contains afterpulses.

saturation behaviour of the SPD, possibly at a high counting rate, the source should provide pulse sets ensuring the correct operation mode of SPD namely, that the light pulses are outside the SPD dead time period. The following source pulse settings are recommended: continuous train generation mode with one pulse in the train and the train repetition period longer than the dead time you have measured.

(c) Change the attenuator setting and observe how the output pulses and count rate change. Observe the count rate saturating and peaking. Note that at higher average optical powers, you may observe a drop in the count rate. This is a normal behaviour indicating detector blinding (which is studied in detail in another lab exercise).

(d) Plot the count rate versus average input optical power, starting from zero optical power. Explain the shape and characteristic points at the curve.

(e) Record two single-shot oscillograms showing multiple pulses in a trace: one in the middle of the linear part of the curve, and another at the maximum count rate. Explain the distribution of pulse times you observe.

Lab report should contain: oscilloscope screenshots similar to Figs. 4 to 6, measured length of the dead time, diagram of your experimental setup, plot of the count rate versus optical power, oscillograms of the linear regime, saturation, and dead time, explanation of the observed effects.

4. Measurement of photon detection efficiency

The efficiency of the SPD will be measured by a calibrated light source method using a pulsed laser [1].

(a) Connect the attenuated light source to the SPD optical input as shown in (Fig. 7). Unlike the scheme suggested in [1], we will not use a beamsplitter.

(b) Set the mean output photon number per pulse around $\mu = 0.2$. At this value, the probability of a pulse containing two or more photons becomes relatively small, as you can verify with Eq. (1), such that it may be neglected. We can then assume we are measuring the detector's response to single-photon pulses.

When calibrating μ, the following considerations should be taken into account. Performing any optical reconnections in the attenuated light source after you have calibrated it is a bad idea, because the fiber-optic connectors vary their insertion loss each time you reconnect them (this variation may be as large as 0.5 dB per connector). Cleaning the connectors carefully helps improve the repeatability, but does not
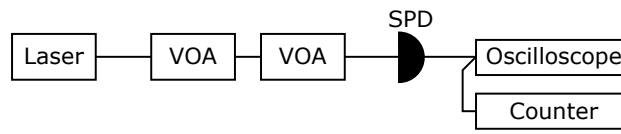
FIG. 7. Suggested setup for measuring photon detection efficiency. VOA, programmable optical attenuator.

    eliminate this problem. Thus you should fully assemble the scheme before performing its calibration, and refrain from reconnecting any connector except the one at the SPD's optical input. You will first use the optical power meter to measure a higher μ at that very point, then change the setting of the programmable optical attenuators to introduce a calibrated amount of attenuation to reduce μ to the desired level. (Here you will rely on the accuracy of relative calibration of the latter devices.) The only optical connector you will thus be reconnecting during the efficiency measurement is at the output of your source and the input of the SPD, i.e., the point at which you are calibrating μ.

    The power meter has a certain minimum sensitivity and cannot accurately measure power below about 10 nW. Please ensure it is measuring power higher than this during the calibration.

(c) Perform the measurement and calculate the SPD efficiency.

(d) Calculate the standard uncertainty in the SPD efficiency. To do that, you need to perform uncertainty propagation on the above equation [9]. (Note that there is a way to make a simpler approximate calculation, which is acceptable if you do it correctly. If in doubt, make the full uncertainty propagation.) Give the final result in the parenthesis notation.

    We remark that besides the statistical uncertainty you calculate in this step, the accuracy of the efficiency measurement is affected by several other factors: the repeatability of the insertion loss at the optical connector, the absolute calibration accuracy of the optical power meter (which can be surprisingly poor, several percent error, for non-metrology-grade power meters like the one you are using), and the relative calibration accuracy of the programmable attenuators (which again can be poor, about 1 dB error, at the higher-attenuation extreme of its range). Accurately accounting for these factors requires background in metrology and is outside the scope of the present course. (If you are really interested to see what it takes, check supplementary information in [10].) Thus we only ask you to estimate the statistical uncertainty, which is a common task in quantum optics experiments.

(e) The uncertainty alone may be significant in this experiment, amounting to a measurement accuracy that is not very satisfactory. Can you think of ways of improving our measurement method to reduce the uncertainty?

Lab report should contain: step-by-step measurement procedure, settings of the devices, calculations and efficiency value with the standard uncertainty.

[1] R. H. Hadfield, Nat. Photonics **3**, 696 (2009).
[2] S. Cova, A. Longoni, A. Andreoni, and R. Cubeddu, IEEE J. Quantum Electron. **19**, 630 (1983).
[3] S. Cova, M. Ghioni, A. Lacaita, C. Samori, and F. Zappa, Appl. Opt. **35**, 1956 (1996).
[4] A. E. Lita, A. J. Miller, and S. W. Nam, Opt. Express **16**, 3032 (2008).
[5] X.-S. Ma, T. Herbst, T. Scheidl, D. Wang, S. Kropatschek, W. Naylor, B. Wittmann, A. Mech, J. Kofler, E. Anisimova, V. Makarov, T. Jennewein, R. Ursin, and A. Zeilinger, Nature **489**, 269 (2012).
[6] Uncertainty in parenthesis, `https://physics.stackexchange.com/questions/158589/uncertainty-in-parenthesis`, visited 5 Sep 2020.
[7] Poisson distribution, `https://en.wikipedia.org/wiki/Poisson_distribution`, visited 22 Apr 2022.
[8] 68–95–99.7 rule, `https://en.wikipedia.org/wiki/68%E2%80%9395%E2%80%9399.7_rule`, visited 22 Apr 2022.
[9] Propagation of uncertainty, `https://en.wikipedia.org/wiki/Propagation_of_uncertainty`, visited 28 Aug 2020.
[10] F. Marsili, V. B. Verma, J. A. Stern, S. Harrington, A. E. Lita, T. Gerrits, I. Vayshenker, B. Baek, M. D. Shaw, R. P. Mirin, and S. W. Nam, Nat. Photonics **7**, 210 (2013).

Single-photon detectors for optical quantum information applications

Robert H. Hadfield

The past decade has seen a dramatic increase in interest in new single-photon detector technologies. A major cause of this trend has undoubtedly been the push towards optical quantum information applications such as quantum key distribution. These new applications place extreme demands on detector performance that go beyond the capabilities of established single-photon detectors. There has been considerable effort to improve conventional photon-counting detectors and to transform new device concepts into workable technologies for optical quantum information applications. This Review aims to highlight the significant recent progress made in improving single-photon detector technologies, and the impact that these developments will have on quantum optics and quantum information science.

One of Einstein's key contributions to modern science was to recognize that light is fundamentally composed of individual packets of energy, now referred to as photons[1,2]. The energy of a single photon in the visible or near-infrared range is around 10^{-19} J. A single-photon detector is an extremely sensitive device capable of registering these quantum objects. Single-photon detectors now support and enable a host of applications at the frontiers of science and engineering. Conventional single-photon detectors are based on photomultipliers and avalanche photodiodes, and are used in a wide range of time-correlated single-photon counting (TCSPC) applications[3]. However, the major driver for single-photon detector development has been the rapidly expanding interest in optical quantum information (QI) applications[4]. Quantum information technologies use individual quantum objects (such as photons) to encode and manipulate information[5], and promise to have a dramatic technological impact in the twenty-first century[6]. The most mature of these innovations is quantum key distribution (QKD)[7,8], the most secure form of communication yet devised, and is now at the point of becoming commercially viable. Perhaps the most ambitious photonic QI application is linear optical quantum computing (LOQC)[9–11] — a scalable paradigm for QI processing and computation. LOQC remains a distant but tantalizing objective, and significant efforts have been mobilized worldwide towards this goal. A major reason that advanced QI technologies such as LOQC are so difficult to realize is the stringent demands these applications place on optical components such as single-photon detectors[12]. Significant improvements are required in terms of their signal-to-noise ratio, detection efficiency, spectral range and ability to resolve photon number (the number of photons reaching the detector simultaneously). Scientists and engineers around the world have taken up this challenge. Their efforts have led to considerable improvements in conventional single-photon detectors and to the emergence of new photon-counting technologies.

Quantifying the performance of single-photon detectors

The performance of a single-photon detector should be assessed[8,13] in terms of its spectral range, dead time, dark count rate, detection efficiency, timing jitter and ability to resolve photon number. We will consider these characteristics in detail, in particular with reference to the requirements of different optical QI applications. Spectral range, dead time, dark count rate, detection efficiency and timing jitter are all important general benchmarks for single-photon detectors, and the ability to resolve photon number is required

in advanced QI protocols[10,11]. We will outline accurate measurement strategies for characterizing single-photon detectors and discuss an appropriate 'figure of merit' for quantifying detector performance.

Spectral range. A photon counter is only sensitive over a certain spectral range determined by its constituent materials. The operating wavelength of interest depends on the particular application. For free-space optical applications (either bench-top quantum optics experiments[13] or line-of-sight QKD through the atmosphere[8]) visible or near-infrared wavelengths are used to exploit the best commercially available detectors. Losses in optical fibre are lowest at a wavelength of 1,550 nm, making this wavelength a clear choice for long distance QKD in optical fibres[8]. Other advanced optical components such as on-chip waveguides are also tailored to telecommunications wavelengths. There is therefore considerable interest in the field of QI in telecommunications-wavelength detectors.

Dead time. The detector 'dead time' or recovery time, τ, is the time interval that follows the absorption of a photon, during which the detector is unable to reliably register a second photon. The factors influencing τ depend strongly on the detector type. In many cases, the measured value of τ is that of the bias circuit or the counting electronics, rather than the detector element itself. In semiconductor single-photon detectors, τ is deliberately lengthened to suppress afterpulsing, the spontaneous retriggering of the detector after an initial detection event. The dead time limits the maximum count rate of the detector but not the clock rate of the experiment, which can be much higher because TCSPC experiments are typically operated in the regime where the number of detected photons per clock cycle is much less than one.

Dark count rate. Most practical detector technologies have a finite probability of recording false counts, known as dark counts, dark noise or dark current, which arise either due to the materials properties of the detector, the biasing conditions or the susceptibility to external noise. In practical applications, the dark count rate of interest, D, is that measured with the detector embedded in the experiment — dark count measurements of completely shielded detectors can give unrealistic values that are of little help or guidance to potential users. D is usually given by a rate in hertz, but can be mitigated by gating or time-stamping the detection events. The minimum time interval for gating or time-stamping is set by the timing jitter of the detector.

Scottish Universities Physics Alliance and the School of Engineering and Physical Sciences, Heriot-Watt University, Edinburgh EH14 4AS, UK.
e-mail: r.h.hadfield@hw.ac.uk

Box 1 | Measurement of the detection efficiency, η

Measurement of η, the probability of registering a count if a photon arrives at the detector, can be achieved through two distinct methods.

Calibrated light source method

This method (Fig. B1a) relies on calibrating a light source with a power meter and then attenuating the output heavily to determine the incident power P. The number of incident photons per second is given by $R_{incident} = P\lambda/hc$, where λ is the wavelength and hc/λ is the energy per photon. One would expect that measurements using either pulsed or continuous wave (CW) sources should give the same reading. If, however, the detector recovery is affected by even a weak photon flux (as in the case of many semiconductor detectors where photon absorption affects the occupancy of low-lying trap states), then a pulsed measurement, in which the frequency f is lower than $1/\tau$ (where τ is the detector dead time), is the more reliable of the two measurements. Moreover, detector saturation or afterpulsing is easier to detect in a pulsed measurement. However, it is important to note that optical power meters are often only accurately calibrated for CW input power.
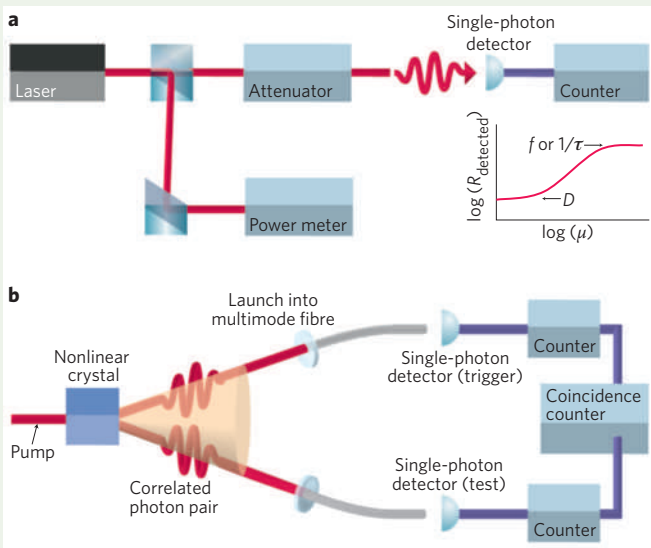
Figure B1 | Determination of single-photon detector efficiency.
a, Calibrated laser method. A continuous wave or pulsed laser is measured using a calibrated power meter. A series of calibrated attenuators are then used to reduce the photon flux μ to less than one photon per time interval. The count rate of the detector $R_{detected}$ is recorded over a range of values of μ. Typically, $R_{detected}(\mu)$ will be of the form shown in the inset. In the continuous-wave case, $R_{detected}$ will saturate at the inverse of the detector (or counter) recovery time, τ. In the pulsed case, saturation should occur at the repetition frequency of the laser, f. At low values of μ, the residual count rate is due to dark counts in the detector. At intermediate values of μ, the signature of a single-photon detector is that $R_{detected}$ is proportional to μ. **b**, Correlated photon method. This method avoids the need for a calibrated power meter. A pair of correlated photons is produced from spontaneous parametric down-conversion source. The signal and idler photons are routed to the test and trigger detectors, then the respective count rates — including coincidences between the two channels — are recorded. The detection efficiency of the test detector channel is given by the coincidence rate divided by the count rate at the trigger detector.

Measurement using a CW source. For the case of a CW measurement of η, the fundamental time interval is set by τ. The mean photon number per time interval, μ, is

$$\mu = R_{incident}\,\tau$$

For a Poissonian light source in the limit of $\mu\eta \ll 1$, the count rate of an ideal detector is

$$R_{detected} = \frac{1}{\tau}(1-\exp(-\mu\eta)) \approx \frac{\mu\eta}{\tau}$$

The true count rate due to actual photodetection events, $R'_{detected}$, can be derived by correcting for the separately measured dark count rate D and the dead time τ, giving

$$R'_{detected} = \left(\frac{R_{detected}}{1 - R_{detected}\tau} - \frac{D}{1 - D\tau}\right)$$

The detection efficiency is therefore

$$\eta = \frac{R'_{detected}}{R_{incident}} = \tau\left(\frac{R_{detected}}{1 - R_{detected}\tau} - \frac{D}{1 - D\tau}\right)\bigg/\mu$$

The parameters η, μ and τ can be determined by analysing a plot of $R_{detected}$ against the photon flux per time interval, μ (Fig. B1a, inset). At low numbers of detected photons ($\mu\eta \ll 1$) the signature of single-photon sensitivity is that $R_{detected} \propto \mu$, but a detector triggered by a two-photon event would give $R_{detected} \propto \mu^2$.

Measurement using a pulsed source. For a pulsed source of frequency $f \ll 1/\tau$ and a mean photon number per pulse μ,

$$R_{incident} = \mu f$$

$$R_{detected} = f(1-\exp(-\mu\eta)) \approx \mu\eta f$$

One would therefore expect the detector count rate to saturate under high photon flux at the clock rate of the source. In this case, the detection efficiency is given by

$$\eta = \frac{R_{detected}}{R_{incident}} = \left(\frac{R_{detected}}{1 - R_{detected}\tau} - \frac{D}{1 - D\tau}\right)\bigg/\mu f$$

Correlated photon method

The correlated photon method (Fig. B1b) uses a source of correlated photons to characterize the detector[14,15]. Remarkably, this elegant technique requires no calibrated power meter. Photons from the pump laser of frequency ω_p are converted into signal and idler photons of frequency ω_s and ω_i, respectively, by spontaneous parametric down-conversion, which conserves energy and momentum such that $\omega_p = \omega_s + \omega_i$. The signal and idler photons are directed to the test and trigger detectors. Coincidences between the two detector channels are recorded. N is the number of photon pairs emitted in the counting period. The counts in the test and trigger detector are given by $N_1 = \eta_1 N$ and $N_2 = \eta_2 N$, respectively, and the total coincidence counts are given by $N_{coinc} = \eta_1\eta_2 N$. The detection efficiency of the test detector is therefore $\eta_1 = N_{coinc}/N_2$, which is independent of the efficiency of the trigger channel. This technique, however, only gives the overall efficiency of the test detector channel, which is problematic for small ($<100\ \mu$m diameter) detectors.
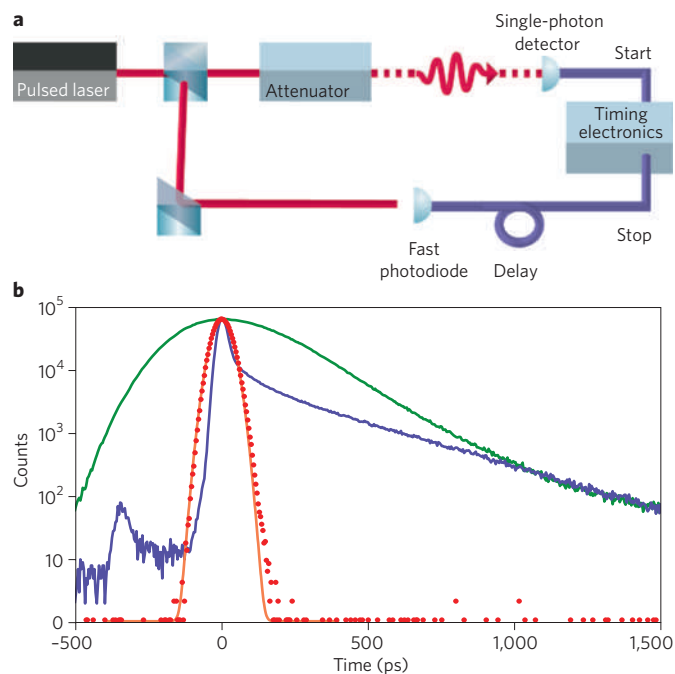
Figure 1 | Measurement of timing jitter. a, The timing jitter of a single-photon detector is the variation in delay between the absorption of a photon and the generation of an output electrical pulse. To measure the timing jitter accurately, a picosecond pulsed laser and high-resolution timing electronics are required to ensure that the dominant jitter is that of the detector. A count on the single-photon detector triggers the 'start' for the timing electronics, and the delayed clock pulse from the laser signals the 'stop'. A histogram of start–stop time intervals is accumulated over multiple clock cycles, giving the instrument response of the single-photon detector. **b**, Instrument responses of three types of single-photon detector, measured using a mode-locked Ti:Sapphire laser at 780 nm and picosecond timing electronics. The thick junction Si SPAD (green) has a FWHM response of ~400 ps, the shallow junction SPAD (blue) has a FWHM response of ~40 ps but with a strongly asymmetric instrument response function, and the superconducting nanowire single-photon detector (red) has a FWHM response of 68 ps with a Gaussian shape. Part **b** reproduced with permission from ref. 16, © 2009 AIP.

Detection efficiency. The detection efficiency, η, is defined as the overall probability of registering a count if a photon arrives at the detector. In most photon-counting applications a high value of η is certainly desirable, but it is by no means the only practical consideration. The maximum rate at which data can be accumulated in an experiment is governed by both the mean photon number per time interval, μ, and the maximum count rate of the detector, $1/\tau$. Moreover, signal-to-noise considerations are often the true determining factor as to whether an experiment is feasible. The exception is LOQC[9], where an extremely high value of η is essential. For scalable LOQC (even with new cluster-state protocols[10,11]), overall optical losses, including collection from the source, cannot fall below a 67% threshold[12].

Methods of accurately determining η are shown in Box 1, either by using a calibrated light source (Fig. B1a) or correlated photon pairs (Fig. B1b)[14,15]. In the ideal case, the detection efficiency is defined as $\eta = R_{detected}/R_{incident}$, where $R_{detected}$ is the count rate and $R_{incident}$ is the photon arrival rate. The intrinsic quantum efficiency of the actual device is not the paramount concern for the user; the practical detection efficiency η must include the optical coupling efficiency to the detector (through free-space optics or optical fibres). The overall

detection efficiency η of a detector channel is therefore the product of coupling losses, η_{loss}, and the intrinsic quantum efficiency of the detector, η_{det}, such that $\eta = \eta_{loss}\,\eta_{det}$. When η is measured accurately, the dead time τ of the detector and the counting electronics must be considered. Furthermore, the measured count rate of the detector, $R_{detected}$, should be corrected for the finite dark count rate of the detector.

Timing jitter. This is the variation in the time interval between the absorption of a photon and the generation of an output electrical pulse from the detector. A reliable method of measuring Δt for a single-photon detector is shown in Fig. 1a. The full-width half-maximum (FWHM) of the detector instrument response function provides a benchmark for timing jitter. Many detectors have a non-Gaussian instrument response function, however, and this should be taken into account in any detailed analysis. The maximum clock rate of a photon counting experiment (where the mean detected photon number is given by $\eta\mu << 1$) is determined by the timing resolution, and jitter in the source or detector will cause counts to stray into neighbouring clock cycles. Typically, but not always, the detector jitter is dominant. Examples of instrument response functions for three detectors are shown in Fig. 1b[16].

Ability to resolve photon number. Most conventional single-photon detectors can only distinguish between zero or 'one or more' photons[10,17]. This binary response means that a multiphoton pulse triggers the same output signal as a single photon. QI protocols require single-photon states, which are difficult to prepare in practice because attenuated laser pulses obey Poissonian statistics; the probability of producing a photon state $|n\rangle$ is $P(n) = (\mu^n/n!)e^{-\mu}$, where $\mu = \langle n \rangle$ is the mean number of photons per pulse[2]. On-demand single-photon sources for QI applications are a highly active research field. Despite significant progress[18,19], current single-photon sources are imperfect because the second-order correlation function $g^{(2)}(0)$ is non-zero, implying residual multiphoton emission, and also because source emission rates are low (that is, $\mu << 1$). In QKD, multiphoton states represent a security 'loophole' that can be exploited by eavesdroppers. In LOQC[9–11], efficient detection of all photons is crucial for reducing errors. Photon number resolution has been achieved in two ways (Fig. 2). First, certain single-photon detector types (such as superconducting transition edge sensors) intrinsically produce a pulse proportional to the number of photons absorbed (Fig. 2a)[20]. The second method multiplexes conventional detectors[17]. This can be achieved either by combining the output signals of an array of detectors (spatial multiplexing; Fig. 2b)[21,22] or by splitting the multiphoton pulse via a cascade of beamsplitters and then delaying the signals so that they can be detected sequentially by a single detector (time multiplexing; Fig. 2c)[23]. The fidelity with which an n-photon state can be recorded scales as η^n — thus, high-efficiency detectors are desirable for these applications. In a multiplexed photon-number-resolving scheme, it is necessary to have a large number of pixels (or time bins) N, such that $N >> n$, to reduce the possibility that two or more photons were absorbed at any one pixel.

Figures of merit for single-photon detectors. The most widely quoted figure of merit for photodetectors is the noise equivalent power (NEP)[24], and this has proved useful for optical power measurements. For single-photon detectors, the NEP can be given by

$$\frac{h\nu}{\eta}\sqrt{2D}$$

where ν is the photon frequency and h is Planck's constant. The units of NEP are W Hz$^{-1/2}$, and the lowest possible value of NEP is desirable. However, a typical detector (one that does not resolve photon

number) does not measure optical power. Furthermore, NEP does not take into account the timing performance of the detector, nor does it relate D and η in a meaningful way for QI experiments. For example, in a QKD experiment, the detector contribution to the quantum-bit error rate (QBER) is the ratio of the dark count rate to the sifted detected photon rate (the detected rate after comparison of the transmission and receiving bases). Furthermore, D can be reduced by setting the timing window as small as possible. Unless some other factor (the jitter of a single-photon source, for example) has a dominant role, the minimum timing interval is usually limited by the timing jitter of the detector. We can therefore formulate a dimensionless figure of merit that takes all of these factors into consideration, giving

$$H = \eta/(D\Delta t)$$

This is a useful figure not only for QKD but also for a range of TCSPC measurements, both in QI applications and beyond. Better detectors have a higher value of H at the wavelength of interest.

This section has rigorously considered the characterization of single-photon detectors and devised an appropriate figure of merit for optical QI applications. It is crucial to understand these characteristics when selecting the best detector for a given experiment or application. Established and emerging single-photon detectors are compared through these metrics in Table 1.

Established single-photon detector technologies

This section reviews the current performance and future prospects of established single-photon detector technologies. In each case, the operating principle, performance, advantages and disadvantages of each detector type are discussed. Performance characteristics are shown in Table 1. New developments and the potential for further improvements in performance are also noted. Short reviews have been given previously elsewhere[10,17,18], and recent special issues devoted to the topic of photon-counting technologies are also recommended reading[4,25].

Photomultiplier tubes. The most long-established photon-counting technology is the photomultiplier tube (PMT). Single-photon counting in PMTs was demonstrated in 1949[26], and this development heralded the birth of the field of TCSPC[3,27]. Commercial PMT units are now widely available[28,29], and there are continued efforts to improve these devices. Photomultiplier tubes offer large active-areas (diameters of >10 mm) and cover the spectral range of 115–1,700 nm, but with large variations in performance.

A basic PMT consists of a vacuum tube with a photocathode for light absorption, from which electrons are liberated through the photoelectric effect (the energy of the incident photon must exceed the work function of the photocathode material). This single- or few-electron photocurrent is then multiplied by a cascade of secondary electron-emissions from dynodes — a series of electrodes, each one biased at a greater positive voltage than the one before — producing a macroscopic current pulse of >10^6 electrons. Traditional PMTs require large operating voltages around the kilovolt-level, and are fragile and expensive. In certain types of PMT, the excess noise of the multiplication process is sufficiently low to allow some discrimination between one or multiple photons. An alternative configuration is the microchannel plate photomultiplier tube, where glass capillaries are fused in parallel and coated with a secondary electron-emitting material to achieve a single continuous dynode under a bias voltage[30]. Microchannel plate PMTs offer improved timing jitter over basic PMTs, down to ~20 ps at FWHM[30].

Photomultiplier tubes have a maximum efficiency of around 40% at a wavelength of 500 nm in GaAsP photocathodes, and have dark
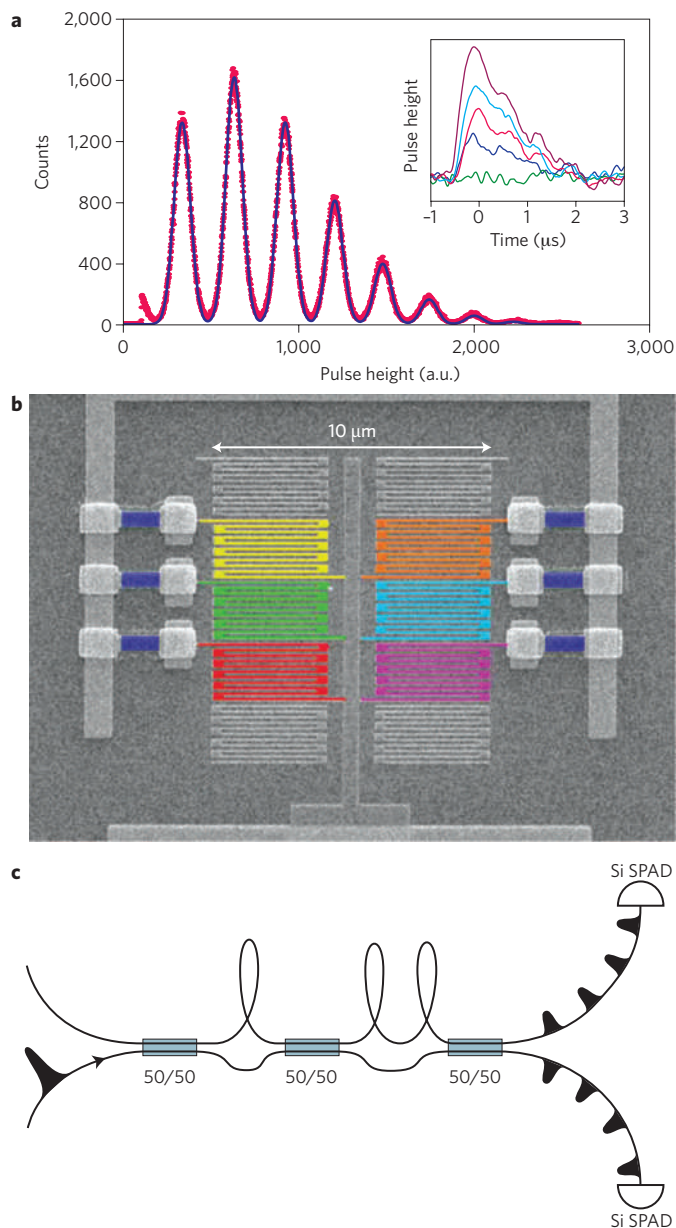
Figure 2 | Photon number resolution. Conventional single-photon detectors give a digital response — an output pulse or 'click' indicates the arrival of one or more photons. Determining the number of photons in a pulse requires a photon-number-resolving detector. **a**, True photon number resolution. Detectors with true photon number resolution give an output that depends on the number of photons absorbed. The superconducting TES is essentially a microcalorimeter — the height of the pulse is proportional to the number of photons at a given wavelength. The figure shows a TES measurement of Poissonian statistics with a mean photon number per pulse of 2.45 at 1,550 nm. The line shows a plot of best-fit to the data, convolving the Poissonian distribution with the energy resolution of the TES. Shown inset is the TES pulse heights for zero to four photons. **b,c**, Conventional single-photon detectors can be combined through spatial or temporal multiplexing to achieve photon number resolution. In spatial multiplexing (**b**), an array of detector pixels (in this case SNSPDs) are broadly illuminated and read-out in parallel. When several pixels are triggered simultaneously, the output pulses are summed. In temporal multiplexing (**c**), The input optical pulse is split via a network of delayed paths such that each photon can be picked out within the dead time interval of the detector pair. Image in **b** reproduced with permission from ref. 22, © 2008 NPG.

Table 1 | Comparison of single-photon detectors.

Detector type	Operation temperature (K)	Detection efficiency, η	Jitter time, Δt (FWHM)	Dark count rate, D (ungated)	Figure of merit	Max. count rate	Resolves photon number?	Class of report
PMT (visible–near-infrared)[31]	300	40% @500 nm	300 ps	100 Hz	1.33×10^7	10 MHz	Yes	†
PMT (infrared)[32]	200	2% @1,550 nm	300 ps	200 kHz	3.33×10^2	10 MHz	Yes	†
Si SPAD (thick junction)[38]	250	65% @650 nm	400 ps	25 Hz	6.5×10^7	10 MHz	No	†
Si SPAD (shallow junction)[41]	250	49% @550 nm	35 ps	25 Hz	5.6×10^8	10 MHz	No	†
InGaAs SPAD (gated)[55]	200	10% @1,550 nm	370 ps	91 Hz	2.97×10^5	10 kHz	No	‡
InGaAs SPAD (self-differencing)[57]	240	10% @1,550 nm	55 ps	16 kHz	1.14×10^5	100 MHz	Yes	‡
Frequency up-conversion[65]	300	9% @1,550 nm	400 ps	13 kHz	1.7×10^4	10 MHz	No	‡
Frequency up-conversion[65]	300	2% @1,550 nm	40 ps	20 kHz	2.5×10^4	10 MHz	No	‡
VLPC[69]	6	88% @694 nm	—	20 kHz	—	—	Yes	§
VLPC*	6	34% @633 nm	270 ps	7 kHz	1.83×10^5	—	Yes	§
TES[76]	0.1	50% @1,550 nm	100 ns	3 Hz	1.67×10^6	100 kHz	Yes	‡
TES[20]	0.1	95% @1,550 nm	100 ns	—	—	100 kHz	Yes	§
SNSPD (meander)[90]	3	0.7% @1,550 nm	60 ps	10 Hz	1.16×10^7	100 MHz	No	‡
SNSPD (new)[87]	1.5	57% @1,550 nm	30 ps	—	—	1 GHz	No	§
QD (resonant tunnel diode)[96]	4	12% @550 nm	150 ns	2×10^{-3} Hz	4×10^9	250 kHz	No	§
QD (field-effect transistor)[93]	4	68% @805 nm	—	—	—	1 Hz	Yes	§

The class of report indicates the conditions under which the detector characteristics were measured; † represents a commercial product specification, ‡ represents the use of the detector in a practical experiment and § represents a measurement of device performance. *Unpublished data, Burm Baek, NIST, USA, 2009.

count rates as low as 100 Hz (ref. 31). The highest reported count rates are up to 10 MHz, and the typical jitter is 300 ps at FWHM[31]. PMTs are now available at telecommunications wavelengths[31] by cooling an InP/InGaAs photocathode to 200 K. Performance is poor compared with visible-wavelength PMTs, however, with a detection efficiency of 2% at 1,550 nm, a dark count rate of 200 kHz and a jitter of ~300 ps at FWHM. Another important development has been the hybrid photodetector, which combines a photocathode with a low-capacitance avalanche photodiode[33]. Hybrid photodetectors require low bias voltages of around 400 V, offer 46% efficiency at 500 nm, and have a timing jitter of 61 ps at FWHM and ~1 kHz dark count rates[33].

Single-photon avalanche photodiodes. Silicon single-photon avalanche photodiodes (Si SPADs; Fig. 3a,b)[34] are now a well-established alternative to PMTs in laboratory quantum optics experiments[13] and free-space QKD systems. These solid-state devices offer low dark count rates, high detection efficiencies and high count rates in the visible to near-infrared range. The long wavelength cut-off is a result of the semiconductor bandgap of Si. In the UV range, absorption occurs before the photon reaches the detection region.

The SPAD is based on an avalanche photodiode structure (a p–n or p–i–n junction). The diode is reverse-biased above the breakdown voltage, and this is known as Geiger mode operation. Carriers generated by photon absorption undergo avalanche gain, triggering a macroscopic breakdown of the diode junction[35]. To harness this

effect in a practical device, the avalanche must be stopped and the device reset by a quenching circuit[34,36].

The highest efficiency commercial devices are based on a thick, 180-μm-diameter high-purity silicon absorber combined with an active quenching circuit and cooling in a single practical module[37,38]. These devices offer single-photon sensitivity in the 400–1,000 nm range and achieve a peak efficiency of 65% at ~650 nm (ref. 38). Dark count rates can be as low as 25 Hz (ref. 36) and the timing jitter is typically ~400 ps at FWHM[16] (Fig. 1b). The operating voltage is low at around 400 V. In Si SPADs the afterpulsing probability is low, with quenching times of approximately 50 ns. Although the excess noise of the multiplication process is too high in SPADs to achieve intrinsic photon number resolution, efforts have been made to achieve this indirectly by exploiting timing walk effects[39] or through spatial-[21] or temporal-multiplexing[23] schemes. Photon emission by hot carriers in an avalanche current ('backflash' photons) can potentially be exploited by eavesdroppers in QKD schemes[40].

A new generation of Si SPAD devices are now available[41]. These are shallow-junction planar devices[42] that have a diameter of 50 μm and require only low operating voltages. The timing is greatly improved to below 40 ps at FWHM (Fig. 1b), but the peak detection efficiency is reduced to 49% at 550 nm.

Silicon SPADs remain an active area of development[43]. Efforts are underway to integrate detector elements directly with quenching circuitry[44], and also to realize millimetre-scale SPAD arrays with low dark counts and minimal crosstalk[45]. The silicon photomultiplier device — an array of SPAD pixels that are read in parallel — can
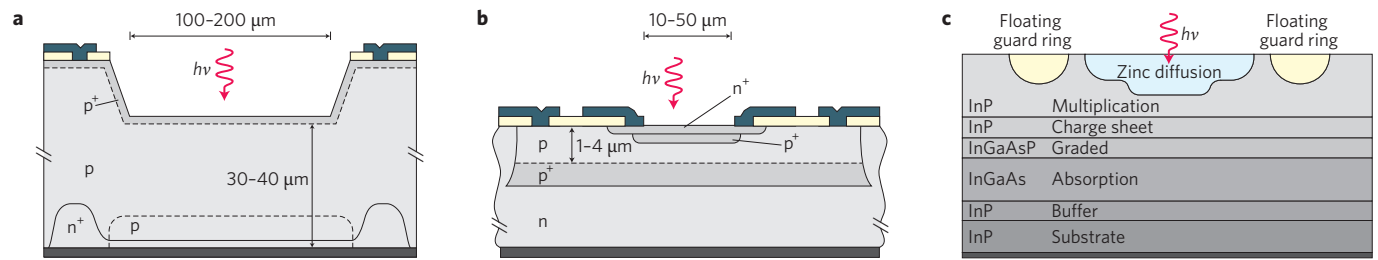
Figure 3 | Established photon-counting technologies based on reverse-biased avalanche photodiodes. a, Thick-junction Si SPAD, a device structure optimized for high detection efficiency and low dark counts. **b**, Shallow-junction planar Si SPAD, a device structure optimized for low timing jitter requiring low bias voltages. **c**, InGaAs/InP SPAD structure, where the use of a smaller-bandgap semiconductor extends single-photon sensitivity to telecommunications wavelengths. Figures reproduced with permission from: **a,b**, ref. 43, © 2004 Taylor & Francis; **c**, ref. 52, © 2006 IEEE.

offer extremely high count rates (~400 MHz) and photon number resolution, but suffer from elevated dark counts[46].

To extend the performance of SPADs to telecommunciations wavelengths ($\lambda = 1{,}310$ nm and 1,550 nm) it is necessary to use lower-bandgap semiconductor materials such as Ge and InGaAs. The best results have been achieved with an InGaAs absorption region and an InP multiplication layer, giving single-photon sensitivities across the 1,000–1,600 nm wavelength range and peak efficiencies of ~20% at 1,550 nm (refs 47–52). The diameter of the active device is ~40 μm, which is suitable for fibre coupling. Owing to materials defects, these devices suffer from dark count rates that are orders of magnitude higher than for their Si counterparts. As a result, InGaAs SPADs are typically operated in gated Geiger mode[51] — the quiescent device is biased beneath the breakdown voltage, then a short (~1 ns) pulse is applied, coincident with the expected arrival of a photon. The dark count rate can be reduced to ~10 kHz (including gating) by cooling to ~200 K, but this reduction in temperature exacerbates afterpuls-ing, causing long detector dead times of around 10 μs and reducing counting rates to ~100 kHz. These devices are now commercially available[53,54] and have allowed fibre QKD systems to reach distances beyond 100 km (ref. 55).

Much of the ongoing effort to improve InGaAs SPAD performance is targeted at QI applications such as QKD. Imaginative biasing and gating schemes, combined with higher-temperature operating schemes to reduce afterpulsing, have led to increased device clock rates[56–58], thus increasing overall bit-rates in QKD[57]. It is also possible to extract multiphoton sensitivity through such methods[59]. Passive quenching at low excess bias can enable free-running operation[60]. Looking ahead, SPADs based on new materials systems such as HgCdTe (ref. 61) may lead to improved long-wavelength performance.

Emerging single-photon detector technologies

We now review a selection of the most promising emerging single-photon detector technologies under consideration for use in QI applications. The operating principle, performance, advantages and disadvantages of each detector are detailed. Where possible, the properties of each emerging technology are compared with those of the established single-photon detector types in Table 1. Instances where these emerging technologies have been implemented in optical QI experiments are highlighted. Recent developments and the potential for future improvements of these technologies are also discussed.

Frequency up-conversion. The goal of frequency up-conversion single-photon detection schemes is to convert a telecommunications-wavelength photon to a shorter wavelength that can be more efficiently detected by a commercial single-photon detector. An example of such a scheme is illustrated in Fig. 4a. The mechanism used is sum-frequency generation in a nonlinear optical crystal: a weak signal at frequency ω_{in} is combined with a strong pump signal

at frequency ω_{pump} to yield an output signal at the summation frequency of $\omega_{out} = \omega_{in} + \omega_{pump}$. If sufficient pump power is available, this frequency up-conversion can occur with near-unity efficiency. For example, in periodically poled lithium niobate, using a pump signal at 1,064 nm allows 1,550-nm photons to be converted to 630-nm photons with 90% efficiency[62]. There are several technical challenges in achieving high-efficiency up-conversion. The first is to achieve the desired field strength, either through a coincident pump and signal pulse[63], a continuous-wave pump pulse and a build up cavity[62], or by using a waveguide to concentrate the pump power into a small interaction region[64]. Drawbacks include the difficulty of stabilizing the nonlinear crystal, the presence of nonlinear processes that lead to fluorescence at the up-conversion wavelength (resulting in very high background count rates), and high in- and output coupling losses for waveguides. Up-conversion schemes using thick-junction Si SPADs have shown system detection efficiencies of 46% for 1,550-nm photons, with a jitter of 400-ps at FWHM and dark count rates of 800 kHz (ref. 65). Shallow-junction Si SPADs have also been used, achieving a system detection efficiency of 2% at 1,550 nm, a FWHM jitter of 40 ps and a dark count rate of 20 kHz (ref. 66). Low-jitter hybrid photodetectors have also been used in conjunction with up-conversion[67]. All three variants have been implemented in QKD demonstrations[65–67]. Recent studies have also shown that coherent up-conversion of quantum states is feasible[68], which is an important step for advanced QI applications.

Visible-light photon counters. The visible-light photon counter (VLPC) is a low-temperature semiconductor-based photon counting technology[69–71]. The device offers high-efficiency detection of single photons up to wavelengths of 1 μm, the ability to resolve photon number, good timing resolution and moderate dark counts.

The VLPC is based on an earlier concept called the solid-state photomultiplier, a blocked-impurity-band device based on As-doped silicon, which gives single-photon sensitivity from visible wavelengths up to 30 μm. Solid-state photomultiplier and VLPC devices operate at low voltage through a controlled single-carrier multiplication process, giving rise to a signal that is proportional to the photon number. In a VLPC the gain region and absorber are separate, maximizing the sensitivity in the wavelength range of 400–1,000 nm. A schematic of the device architechture is shown in Fig. 4b. An electron–hole pair is generated in the undoped (intrinsic) Si absorber region, and the resulting hole triggers an avalanche in the gain region through interaction with As impurity levels. This single-carrier multiplication process only requires a small bias voltage of 6–7.5 V, but the device temperature must be carefully tuned to around 6 K to achieve optimal performance. As the avalanche is confined to a 20-μm-wide filament and the overall device diameter is 1 mm, two photons can produce distinct concurrent avalanches if the focal spot is large. The low excess noise of the multiplication
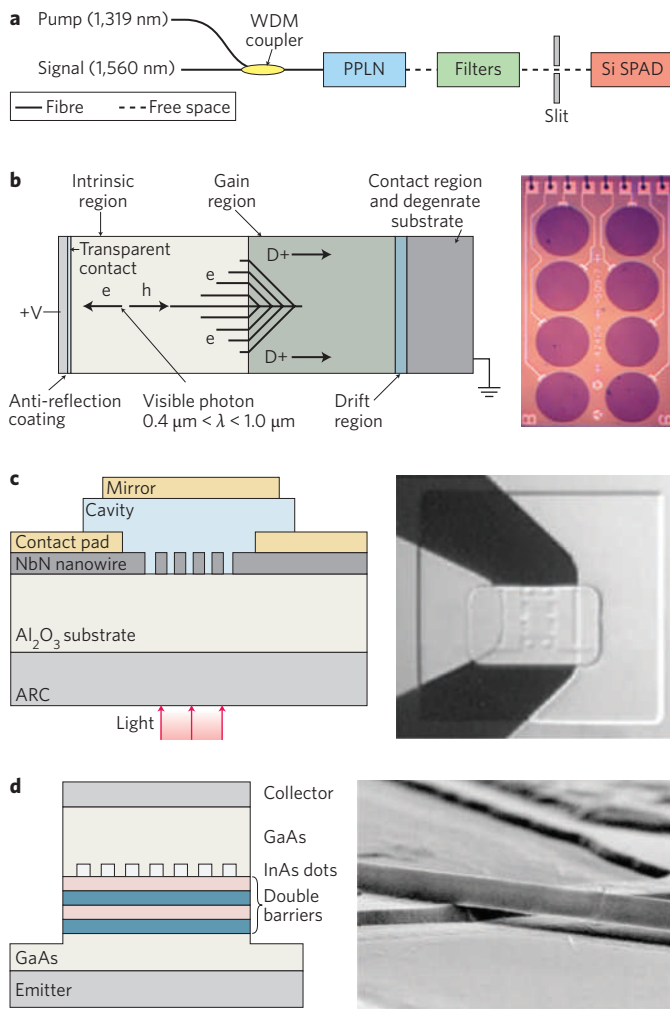
Figure 4 | Emerging single-photon detectors: a selection of promising technologies. a, Frequency up-conversion detector. A 1,560-nm photon is converted to a 715-nm photon through sum frequency generation in a periodically poled lithium niobate waveguide, and is detected by a Si SPAD. WDM, wavelength-division multiplexer. **b**, Visible-light photon counter. This is a low-temperature semiconductor technology. The single-carrier multiplication process allows for photon number resolution. A device schematic (left) and an optical micrograph of eight VLPC pixels (right) are shown. **c**, A next-generation superconducting nanowire single-photon detector, showing the device schematic (left) and optical micrograph (right). A niobium nitride (NbN) SNSPD is embedded in a resonant cavity to enhance the detection efficiency. ARC, anti-reflection coating. **d**, A detector based on a quantum dot resonant tunnelling diode, showing the device schematic (left) and a scanning electron micrograph of the cross-wire device structure (right). Figures reproduced with permission from: **a**, ref. 65, © 2005 IOP; **b**, ref. 71, © 2003 IEEE; **c**, ref. 87, © 2005 OSA; **d**, ref. 96, © 2005 APS.

process is close to the theoretical minimum, allowing up to five photons to be resolved[70,71]. VLPC detection efficiencies of up to 88% at 694 nm and 93% in the infrared have been observed, neglecting coupling losses and spectral filtering[69]. The dark count rate is ~20 kHz at the maximum detection efficiency. The dead time of the VLPC is ~100 ns, and therefore the upper limit to the count rate is ~100 kHz. The jitter of these devices has recently been measured at 633 nm (unpublished data, Burm Baek, NIST, USA, 2009), and the lowest value obtained is 250 ps at FWHM in the dark count

range of 6.9–25 kHz, with a maximum fibre-coupled detection efficiency of 40%.

VLPCs are highly desirable for QI applications requiring high detection efficiency and photon number resolution. So far, VLPCs have been successfully used in studies of photon statistics in non-classical parametric down-conversion sources[72].

Superconducting transition-edge sensors. Superconducting transition-edge sensors (TESs) are low-temperature devices that offer very-high-efficiency single-photon detection with photon-number-resolving capability and low dark count rates. In a TES, the detector element is a superconducting film on the cusp of the superconducting transition, where any change in temperature will cause an abrupt change in resistance[73]. The absorption of an incident photon heats the device, causing the voltage-biased detector to draw a current that can be read out using a SQUID amplifier. The signal is proportional to the energy of the photon or, at fixed wavelength, the photon number[74]. This intrinsic ability to resolve photon number is illustrated in Fig. 2a[20]. These detectors operate at temperatures of around 100 mK and therefore require sophisticated cooling technology. The current tungsten-based detectors have a detection efficiency of 20%[75] — which increases to 95% efficiency at 1,550 nm (ref. 20) when they are embedded in a optical cavity structure — and have negligible dark counts. In practical implementations, the effective dark count rate may rise due to room-temperature blackbody radiation[76]. This effect can be mitigated by filtering, but this reduces the detection efficiency. The photon-number-resolving capabilities are excellent — up to eight photons can be resolved clearly[20]. High-efficiency devices for the near-infrared (~850 nm) have also recently been reported[77]. The timing properties of TES detectors are relatively poor, with jitter times of around 100 ns at FWHM. The dead time of the detector is limited by the thermal time constant of the detector element, and is typically ~1 μs. Faster detectors, with dead times around 100 ns, can be fabricated using films of higher transition temperatures[77], but these devices require faster SQUID read-out electronics.

TES detectors have so far been successfully implemented in quantum optics experiments[78] and long-distance QKD[76,79]. Owing to their near-unity detection efficiency and ability to resolve photon number, these detectors are highly promising candidates for fundamental tests of quantum mechanics, LOQC and optical quantum metrology applications.

Superconducting nanowire single-photon detectors Superconducting nanowire single-photon detectors (SNSPDs) offer single-photon sensitivity from visible to mid-infrared wavelengths, low dark counts, short recovery times and low timing jitter.

The detector element itself is a 100-nm-wide nanowire that is patterned by electron-beam lithography in an ultrathin niobium nitride superconducting film[80]. It operates in the temperature range of 1.5–4 K, well below the superconducting transition temperature of the niobium nitride film. The material is chosen because of its exceptionally fast photoresponsive properties[81]. The superconducting wire is biased just below its critical current, which is the point at which the wire becomes resistive. When a photon strikes the wire, a local resistive hotspot is formed, perturbing the current distribution and thus triggering a fast voltage-pulse[80] that can then be amplified and measured. The detection efficiency and dark count rate are both dependent on the bias point, with the dark count rate rising more steeply close to the critical current.

Current devices consist of a 'meander wire'[82] that covers an area of up to 20 μm × 20 μm (ref. 83) to achieve a high coupling efficiency between the nanowire and a single-mode optical fibre. The device is embedded in a microwave coplanar waveguide to facilitate the read-out of fast voltage pulses. Fabrication of large-area detectors is challenging

because the wire must be completely uniform along its length — a constriction at any point in the wire will negate the sensitivity of the rest of the detector[84]. The use of a single, long meander wire increases the overall inductance, lengthening the detector dead time[85] to around 10 ns for large-area detectors[86] — although this is a significant increase, it is still an order of magnitude faster than conventional photon counters. The intrinsic efficiency of small-area (3 μm × 3.3 μm) single-layer SNSPDs is as high as 20% at 1,550 nm, which is close to the expected absorption of the material[87]. Fibre-coupled large-area SNSPDs offer practical detection efficiencies of >1% at 1,550 nm, with dark count rates below 1 kHz (refs 83,86). The timing jitter of the device is extremely good (compared with Si SPADs[16]; Fig. 1b) — 65 ps at FWHM can be achieved in large-area devices[19], and 30 ps FWHM or less in small-area devices[87].

An exciting aspect of this technology is that considerable performance improvements are well within reach. SNSPDs have been integrated into low-Q optical cavity structures with back-reflector mirrors (the device architecture and an optical micrograph are shown in in Fig. 4c). This improves the intrinsic detection efficiency to as much as 57% for small-area devices[87]. The addition of a cavity does not degrade the timing performance of the detector. A limitation of current niobium nitride devices is that they must be grown on lattice-matched substrates (sapphire or MgO) at high temperatures (>600 °C). The demonstration of high-quality devices on alternative substrates, such as NbTiN deposited at room temperature on Si (ref. 88), will increase the versatility of this detector technology. Multipixel SNSPD devices have also recently been demonstrated[20,89]. Such devices provide spatially multiplexed photon number resolution, allowing larger detector areas to be achieved with both low timing jitter and short recovery times.

Basic meander-type SNSPDs[82] have now been widely implemented in optical QI applications. Fibre-coupled SNSPDs can be integrated into practical, closed-cycle refrigerator systems operating at ~3 K (ref. 86), widening the range of accessible applications. SNSPDs have had a major impact in the field of QKD, leading to record transmission distances and bit-rates in optical fibres[90]. As next-generation high-efficiency devices[87] become available, the importance of these detectors in optical QI science and technology is expected to continue increasing.

Single-photon detectors based on quantum dots and semiconductor defects. Another new class of devices utilize the trapping of charge in defects to achieve single-photon detection. Semiconductor heterostructures based on III–V compounds form the basic device architecture: either quantum dots (QDs) embedded in the material[91–97] or intrinsic defects[98] are exploited to achieve trapping. QDs are favoured as they can be controllably placed within the heterostructure to maximize internal efficiency and signal uniformity. Two main detection schemes have been realized. The first relies on a photoconductive gain mechanism that involves trapping charge in a defect or QD layer, which alters the conductance in a field-effect transistor structure[91–95,98]. These types of device have been operated at count rates of up to 400 kHz (ref. 92), and a high internal efficiency of up to 68% has been demonstrated at 805 nm (ref. 93). Resolution of up to three photons in such devices has also been shown[94,95].

The second scheme relies on photo-absorption in a QD, which alters the tunnelling probability in a resonant tunnel diode structure[96,97]. Quantum-dot-resonant tunnel diode devices have demonstrated single-photon detection efficiencies of up to 12% at 550 nm, jitter of 150 ns and very low dark count rates (down to 2×10^{-3} Hz). Devices of this type have recently been realized at telecommunications wavelengths[97].

These devices are currently at an early stage of development; the only successful demonstrations have been carried out at cryogenic temperatures (~4 K). Low dark count rates have been reported.

Device performance seems to be limited by large timing jitter, and practical detection efficiencies are low because of the micrometre-scale device areas. Improvements are anticipated, however, and if sources of noise can be eliminated, higher temperature operation may be possible. Furthermore, resonant cavities may boost device efficiency. This class of detectors offers intriguing prospects for future QIP technologies. There is a clear compatibility with III–V semiconductor QD single-photon sources[19]. There is also potential for these types of structures to achieve spin-preserving photodetection[99]; transferring photon polarization to electron or hole spin is one possible candidate for emerging quantum memory and repeater technologies.

Outlook and conclusion

This review has summarized key performance parameters and defined a figure of merit for single-photon detectors in optical quantum information applications. The current performance of established and emerging detector technologies has also been reviewed. Semiconductor-based detectors such as single-photon avalanche diodes have attained a high level of maturity and are widely used in laboratory quantum optics and quantum information experiments. There are ongoing efforts to improve the performance of single-photon avalanche diodes at telecommunications wavelengths, for quantum information applications such as long-distance quantum key distribution in optical fibre. To meet the demands of new quantum information applications, a host of new single-photon detector technologies are being rapidly devised, developed, evaluated and deployed. As a result, low-temperature detectors with infrared sensitivity, excellent timing resolution and a high signal-to-noise ratio, such as superconducting nanowire single-photon detectors, have set new benchmarks in long distance, high-bit-rate quantum key distribution. Visible-light photon counters and superconducting transition-edge sensors now offer near-unity detection efficiency and the ability to resolve photon number, which are both prerequisites for scalable linear optical quantum computing. These improvements in detector technology are therefore having an immediate scientific impact, allowing the frontiers of quantum information science and quantum optics to be pushed forward. Moreover, these new single-photon detector technologies are poised to have a profound impact in a range of fields far beyond that of quantum information. There is widespread demand for improved single-photon detectors, particularly at infrared wavelengths; such technologies are eagerly awaited in fields as diverse as astronomy, laser ranging, remote sensing, classical communications and biomedical imaging.

References

1. Einstein, A. On a heuristic point of view about the creation and conversion of light. *Ann. Phys. (Leipz.)* **17,** 132–148 (1905).
2. Loudon, R. *Quantum Theory of Light* 3rd edn, Ch. 1 (Oxford Univ. Press, 2000).
3. Becker, W. *Advanced Time-Correlated Single Photon Counting Techniques* Ch. 2 (Springer, 2005).
4. Migdall, A. Introduction to journal of modern optics special issue on single-photon: detectors, applications, and measurement methods. *J. Mod. Opt.* **51,** 1265–1266 (2004).
5. Nielsen, M. A. & Chuang, I. L. *Quantum Computation and Quantum Information* Ch. 1 (Cambridge Univ. Press, 2000).
6. Zoller, P. *et al.* Quantum information processing and communication. *Eur. Phys. J. D* **36,** 203–228 (2005).
7. Bennett, C. H. & Brassard, G. in *Proc. IEEE Int. Conf. Computers, Systems and Signal Processing, Bangalore* 175–179 (1984).
8. Gisin, N., Ribordy, G., Tittel, W. & Zbinden, H. Quantum cryptography. *Rev. Mod. Phys.* **74,** 145–195 (2002).
9. Knill, E., Laflamme, R. & Milburn, G. J. A scheme for efficient quantum computation with linear optics. *Nature* **409,** 46–52 (2001).
10. Kok, P. *et al.* Linear optical quantum computing with photonic qubits. *Rev. Mod. Phys.* **79,** 135–175 (2007).
11. O'Brien, J. L. Optical quantum computing. *Science* **318,** 1567–1570 (2007).

12. Varnava, M., Browne, D. E. & Rudolph, T. How good must single photon sources and detectors be for efficient linear optical quantum computation? *Phys. Rev. Lett.* **100**, 060502 (2008).
13. Bachor, H.-A. & Ralph, T. C. *A Guide to Experiments in Quantum Optics* 2nd edn, Ch. 7 (Wiley-VCH, 2004).
14. Rarity, J. G., Ridley, K. D. & Tapster, P. R. Absolute measurement of detector quantum efficiency using parametric downconversion. *Appl. Opt.* **26**, 4616–4619 (1987).
15. Ware, M. & Migdall A. Single-photon detector characterization using correlated photons: the march from feasibility to metrology. *J. Mod. Opt.* **51**, 1549–1557 (2004).
16. Stevens, M. J. *et al.* Fast lifetime measurements of infrared emitters using a low-jitter superconducting single-photon detector. *Appl. Phys. Lett.* **89**, 031109 (2006).
17. Silberhorn, C. Detecting quantum light. *Contemp. Phys.* **48**, 143–156 (2007).
18. Kumar, P. *et al.* Photonic technologies for quantum information processing. *Quantum Inf. Process.* **3**, 215–231 (2004).
19. Shields, A. J. Semiconductor quantum light sources. *Nature Photon.* **1**, 215–223 (2007).
20. Lita, A. E., Miller, A. J. & Nam, S. W. Counting near-infrared single-photons with 95% efficiency. *Opt. Express* **16**, 3032–3040 (2008).
21. Jiang, L. A., Dauler, E. A. & Chang, J. T. Photon-number-resolving detector with 10 bits of resolution. *Phys. Rev. A* **75**, 062325 (2007).
22. Divochiy, A. *et al.* Superconducting nanowire photon-number-resolving detector at telecommunication wavelengths. *Nature Photon.* **2**, 302–306 (2008).
23. Achilles, D., Silberhorn, C., Sliwa, C., Banaszek, K. & Walmsley, I. A. Fiber-assisted detection with photon-number resolution. *Opt. Lett.* **28**, 2387–2389 (2003).
24. Donati, S. *Photodetectors: Devices, Circuits and Applications* Ch. 3 (Prentice Hall, 2000).
25. Cheung, J., Migdall, A. & Rastello, M.-L. Single-photon sources, detectors, applications and measurement methods. *J. Mod. Opt.* **56**, 139–140 (2009).
26. Morton, G. A. Photomultipliers for scintillation counting. *RCA Rev.* **10**, 525–553 (1949).
27. Poultney, S. K. Single-photon detection and timing: experiments and techniques. *Adv. Electron. El. Phys.* **31**, 39–117 (1972).
28. http://jp.hamamatsu.com/.
29. http://www.burle.com/index.html.
30. Kume, H., Koyama, K., Nakatsugawa, K., Suzuki, S. & Fatlowitz, D. Ultrafast microchannel plate photomultipliers. *Appl. Opt.* **27**, 1170–1178 (1988).
31. http://jp.hamamatsu.com/resources/products/etd/pdf/m-h7422e.pdf.
32. http://jp.hamamatsu.com/resources/products/etd/pdf/NIR-PMT_APPLI_TPMO1040E02.pdf.
33. Fukasawa, A., Haba, J., Kageyama, A., Nakazawa, H. & Suyama, M. High speed HPD for photon counting. *IEEE Trans. Nucl. Sci.* **55**, 758–762 (2008).
34. Cova, S., Longoni, A. & Andreoni, A. Towards picoseconds resolution with single-photon avalanche diodes. *Rev. Sci. Inst.* **52**, 408–412 (1981).
35. Haitz, R. H. Mechanisms contributing to the noise pulse rate of avalanche diodes. *J. Appl. Phys.* **36**, 3123–3131 (1965).
36. Brown, R. G. W., Jones, R., Rarity, J. G. & Ridley, K. D. Characterization of silicon avalanche photodiodes for photon correlation measurements 2: Active quenching. *Appl. Opt.* **26**, 2383–2389 (1987).
37. Daudet, H. *et al.* Photon counting techniques with silicon avalanche photodiodes. *Appl. Opt.* **32**, 3894–3900 (1993).
38. http://optoelectronics.perkinelmer.com/content/RelatedLinks/SpecificationSheets/SPC_PhotoDetectors.pdf.
39. Blazej, J. Photon number resolving in Geiger mode avalanche photodiode photon counters. *J. Mod. Opt.* **51**, 1491–1498 (2004).
40. Kurtsiefer, C., Zarda, P., Mayer, S. & Weinfurter, H. The breakdown flash of silicon avalanche photodiodes — a back door for eavesdropper attacks? *J. Mod. Opt.* **48**, 2039–2047 (2001).
41. http://www.microphotondevices.com/products_pdm.asp.
42. Cova, S., Lacaita, A., Ghioni, M., Ripamonti, G. & Louis, T. A. 20-ps timing resolution with single-photon avalanche diodes. *Rev. Sci. Inst.* **60**, 1104–1110 (1989).
43. Cova, S., Ghioni, M., Lotito, A., Rech, I. & Zappa, F. Evolution and prospects for single-photon avalanche diodes and quenching circuits. *J. Mod. Opt.* **51**, 1267–1288 (2004).
44. Zappa, F., Ghioni, M., Cova, S., Samori, C. & Giudice, A. C. An integrated active-quenching circuit for single-photon avalanche diodes. *IEEE Trans. Instr. Meas.* **49**, 1167–1175 (2000).
45. Rech, I. *et al.* Optical crosstalk in single photon avalanche diode arrays: a new complete model. *Opt. Express* **16**, 8381–8394 (2008).
46. Eraerds, P., Legré, M., Rochas, A., Zbinden, H. & Gisin, N. SiPM for fast photon-counting and multiphoton detection. *Opt. Express* **15**, 14539–14549 (2007).

47. Lacaita, A., Zappa, F., Cova, S. & Lovati, P. Single-photon detection beyond 1 μm: performance of commercially available InGaAs/InP detectors *Appl. Opt.* **35**, 2986–2996 (1996).
48. Ribordy, G., Gautier, J.-D., Zbinden, H. & Gisin, N. Performance of InGaAs/InP avalanche photodiodes as gated-mode photon counters. *Appl. Opt.* **37**, 2272–2277 (1998).
49. Rarity, J. G., Wall, T. E., Ridley, K. D., Owens, P. C. M. & Tapster, P. R. Single-photon counting for the 1300–1600-nm range by use of Peltier-cooled and passively quenched InGaAs avalanche photodiodes. *Appl. Opt.* **39**, 6746–6753 (2000).
50. Hiskett, P. A. *et al.* Performance and design of InGaAs/InP photodiodes for single-photon counting at 1.55 μm. *Appl. Opt.* **39**, 6818–6829 (2000).
51. Bethune, D. S. & Risk, W. P. An autocompensating fiber-optic quantum cryptography system based on polarization splitting of light. *IEEE J. Quant. Elect.* **36**, 340–347 (2000).
52. Pellegrini S. *et al.* Design and performance of an InGaAs-InP single-photon avalanche diode detector. *IEEE J. Quant. Elect.* **42**, 397–403 (2006).
53. http://www.princetonlightwave.com/content/PGA-400%20V1.0.pdf.
54. http://www.idquantique.com/products/files/id201-specs.pdf.
55. Gobby, C., Yuan, Z. L. & Shields, A. J. Quantum key distribution over 122 km of standard telecom fiber. *Appl. Phys. Lett.* **84**, 3762–3764 (2004).
56. Namekata, N., Sasamori, S. & Inoue, S. 800 MHz single-photon detection at 1550-nm using an InGaAs/InP photodiode operated with a sine wave gating. *Opt. Express* **14**, 10043–10049 (2006).
57. Dixon, A. R., Yuan, Z. L., Dynes, J. F., Sharpe, A. W. & Shields, A. J. Gigahertz decoy quantum key distribution with 1 Mbit/s secure key rate. *Opt. Express* **16**, 18790–18797 (2008).
58. Thew, R. T., Stucki, D., Gautier, J.-D., Zbinden, H. & Rochas, A. Free-running InGaAs/InP avalanche photodiode with active quenching for single photon counting at telecom wavelengths. *Appl. Phys. Lett.* **91**, 201114 (2007).
59. Kardynał, B. E., Yuan, Z. L. & Shields, A. J. An avalanche-photodiode-based photon-number-resolving detector. *Nature Photon.* **2**, 425–428 (2008).
60. Warburton, R. E., Itzler, M. & Buller, G. S. Free-running room temperature operation of an InGaAs/InP single-photon avalanche diode. *Appl. Phys. Lett.* **94**, 071116 (2009).
61. Rogalski, A., Antoszewski, J. & Faraone, L. Third-generation infrared photodetector arrays. *J. Appl. Phys.* **105**, 091101 (2009).
62. Albota, M. A. & Wong, F. N. C. Efficient single-photon counting at1.55 μm by means of frequency upconversion. *Opt. Lett.* **29**, 1449–1451 (2004).
63. Vandevender, A. P. & Kwiat, P. G. High efficiency single-photon detection via frequency up-conversion. *J. Mod. Opt.* **51**, 1433–1445 (2004).
64. Langrock, C. *et al.* Highly efficient single-photon detection at communication wavelengths by use of upconversion in reverse-proton exchanged periodically poled LiNbO₃ waveguides. *Opt. Lett.* **30**, 1725–1727 (2005).
65. Takesue, H. *et al.* Differential phase shift quantum key distribution experiment over 105 km fibre. *New J. Phys.* **7**, 232–243 (2005).
66. Thew, R. T. *et al.* Low jitter up-conversion detectors for telecom wavelength GHz QKD. *New J. Phys.* **8**, 32–43 (2006).
67. Zhang, Q. *et al.* Megabits secure key rate quantum key distribution. *New J. Phys.* **11**, 045010 (2009).
68. Tanzilli, S. *et al.* A photonic quantum information interface. *Nature* **437**, 116–120 (2005).
69. Takeuchi, S., Kim, J., Yamamoto, Y. & Hogue H. H. Development of a high-quantum-efficiency single-photon counting system. *Appl. Phys. Lett.* **74**, 1063–1065 (1999).
70. Kim, J., Takeuchi, S., Yamamoto, Y. & Hogue, H. H. Multiphoton detection using visible light photon counter. *Appl. Phys. Lett.* **74**, 902–904 (1999).
71. Waks, E. *et al.* High-efficiency photon-number detection for quantum information processing. *IEEE J. Sel. Top. Quant.* **9**, 1502–1511 (2003).
72. Waks, E., Diamanti, E., Sanders, B. C., Bartlett, S. D. & Yamamoto, Y. Direct observation of nonclassical photon statistics in parametric down-conversion. *Phys. Rev. Lett.* **92**, 113602 (2004).
73. Cabrera, B. *et al.* Detection of single infrared, optical and ultraviolet photons using superconducting transition edge sensors. *Appl. Phys. Lett.* **73**, 735–737 (1998).
74. Miller, A. J., Nam, S. W., Martinis, J. M. & Sergienko, A. V. Demonstration of a low-noise near-infrared photon counter with multiphoton discrimination. *Appl. Phys. Lett.* **83**, 791–793 (2003).
75. Rosenberg, D., Lita, A. E., Miller, A. J. & Nam, S. W. Noise-free high-efficiency photon-number-resolving detectors. *Phys. Rev. A* **71**, 061803 (2005).
76. Rosenberg, D. *et al.* Long-distance decoy-state quantum key distribution in optical fiber. *Phys. Rev. Lett.* **98**, 010503 (2007).
77. Fukuda, D. *et al.* Photon number resolving detection with high speed and high quantum efficiency. *Metrologia* **46**, S288–S292 (2009).
78. Di Giuseppe, G. *et al.* Direct observation of photon pairs at a single output port of a beam-splitter interferometer. *Phys. Rev. A* **68**, 063817 (2003).

79. Rosenberg, D. *et al.* Quantum key distribution at telecom wavelengths with noise-free detectors. *Appl. Phys. Lett.* **88,** 021108 (2006).
80. Gol'tsman, G. N. *et al.* Picosecond superconducting single-photon optical detector. *Appl. Phys. Lett.* **79,** 705–707 (2001).
81. Il'in, K. S. *et al.* Picosecond hot-electron energy relaxation in NbN superconducting photodetectors. *Appl. Phys. Lett.* **76,** 2752–2754 (2000).
82. Verevkin, A. *et al.* Detection efficiency of large-active-area NbN single-photon superconducting detectors in the ultraviolet to near-infrared range. *Appl. Phys. Lett.* **80,** 4687–4689 (2002).
83. Miki, S. *et al.* Large sensitive-area NbN nanowire superconducting single-photon detectors fabricated on single-crystal MgO substrates. *Appl. Phys. Lett.* **92,** 061116 (2008).
84. Kerman, A. J. *et al.* Constriction-limited detection efficiency of superconducting nanowire single-photon detectors. *Appl. Phys. Lett.* **90,** 101110 (2007).
85. Kerman, A. J. *et al.* Kinetic-inductance-limited reset time of superconducting nanowire photon counters. *Appl. Phys. Lett.* **88,** 111116 (2006).
86. Hadfield, R. H. *et al.* Single photon source characterization with a superconducting single photon detector. *Opt. Express* **13,** 10846–10853 (2005).
87. Rosfjord, K. M. *et al.* Nanowire single-photon detector with an integrated optical cavity and anti-reflection coating. *Opt. Express* **14,** 527–534 (2006).
88. Dorenbos, S. N. *et al.* Low noise superconducting single photon detectors on silicon. *Appl. Phys. Lett.* **93,** 131101 (2008).
89. Dauler, E. A. *et al.* Photon-number-resolution with sub-30-ps timing using multi-element superconducting nanowire single photon detectors. *J. Mod. Opt.* **56,** 364–373 (2009).
90. Takesue, H. *et al.* Quantum key distribution over 40-dB channel loss using superconducting single-photon detectors. *Nature Photon.* **1,** 343–348 (2007).
91. Shields, A. J. *et al.* Detection of single photons using a field-effect transistor gated by a layer of quantum dots. *Appl. Phys. Lett.* **76,** 3673–3675 (2000).
92. Kardynał, B. E. *et al.* Low-noise photon counting with a radio-frequency quantum-dot field-effect transistor. *Appl. Phys. Lett.* **84,** 419–421 (2004).
93. Rowe, M. A. *et al.* Single-photon detection using a quantum dot optically gated field-effect transistor with high internal quantum efficiency. *Appl. Phys. Lett.* **89,** 253505 (2006).
94. Kardynal, B. E. *et al.* Photon number resolving detector based on a quantum dot field effect transistor. *Appl. Phys. Lett.* **90,** 181114 (2007).
95. Gansen, E. J. *et al.* Photon-number-discriminating detection using a quantum-dot, optically gated, field-effect transistor. *Nature Photon.* **1,** 585–588 (2007).
96. Blakesley, J. C. *et al.* Efficient single photon detection by quantum dot resonant tunneling diodes. *Phys. Rev. Lett.* **94,** 067401 (2005).
97. Li, H. W. *et al.* Quantum dot resonant tunneling diode for telecommunication wavelength single photon detection. *Appl. Phys. Lett.* **91,** 073516 (2007).
98. Kosaka, H. *et al.* Photoconduction quantization in a single-photon detector. *Phys. Rev. B* **65,** 201307 (2002).
99. Yablonovitch, E. *et al.* Optoelectronic quantum telecommunications based on spins in semiconductors. *Proc. IEEE* **91,** 761–780 (2003).

Acknowledgements